

Structure and property development of aromatic copolysulfonamide fibers during wet spinning process

Jinchao Yu,¹ Feng Tian,² Shenghui Chen,³ Xiaofeng Wang,³ Yumei Zhang,¹ Huaping Wang¹

¹State Key Laboratory for Modification of Chemical Fibers and Polymer Materials, College of Materials Science and Engineering, Donghua University, Shanghai, 201620, China

²Shanghai Institute of Applied Physics Chinese Academy of Sciences, Shanghai, 201204, China

³Shanghai Tanlon Fiber Co., Ltd, Shanghai, 201419, China

Correspondence to: Y. Zhang (E-mail: zhangym@dhu.edu.cn)

ABSTRACT: The structure and performance changes of aromatic copolysulfonamide (*co*-PSA) fibers that occurred during wet spinning process have been studied. While using different length scale characterization, including scan electron microscopy (SEM), wide-angle X-ray scattering (WAXS), and small-angle X-ray scattering (SAXS), it was found that the molecular chains of *co*-PSA formed an isotropic network during coagulation which further lead to extension and orientation of these chains during the subsequent stretching. As a result, only after heat stretching and heat setting the molecular chains tended to pack into crystal lattice in the fibrils. This gave rise to a much denser structure along the spinning line and the glass transition temperature of *co*-PSA fibers increased a little after heat setting. Before heat stretching, the *co*-PSA fibers were in amorphous state, and only the amorphous orientation was observed within the fibers. After heat stretching at the temperature higher than T_g , the fraction of amorphous region decreased, and the crystal structure formed in the fibers, which became more perfect during heat setting. The structure development during spinning process contributed toward the improvement of thermo-mechanical stability, tenacity and modulus of the *co*-PSA fibers. © 2015 Wiley Periodicals, Inc. *J. Appl. Polym. Sci.* 2015, 132, 42343.

KEYWORDS: aromatic polysulfonamide fibers; structure-property relations; X-ray

Received 8 February 2015; accepted 11 April 2015

DOI: 10.1002/app.42343

INTRODUCTION

Aromatic polysulfonamides (PSAs), belonging to the family of heat resistant polymers, are mostly characterized according to their excellent chemical, thermal stability, larger limit oxygen index (LOI, up to 33%), and low dielectric constants. PSAs play an important role in extensive range of applications such as high-temperature gas filtration, flame-retardant protection, and electrical insulation.^{1,2} In the past few decades, the structure, morphology, and properties of PSA fibers have been reported. The macrostructure of PSA fibers such as cross-section, defects, pores, or densification has attracted much attention. However, the micro-nano structures (e.g., fibrils, crystal structure) of these fibers have not been fully explored.^{3–5}

The effect of spinning technology on the structure and properties of PSA fibers has also been investigated. Banduryan *et al.*⁶ conducted a comparative investigation of the structure and properties of poly (4,4'-diphenylsulfonyl terephthalamide) (*pt*-PSA) fibers prepared by dry- and wet-spinning. The dense and homogeneous morphology was found in the dry-spun fibers while the heterogeneous morphology with microphase

separation has been observed in wet-spun fibers. Banduryan *et al.*⁷ and Muraveva and Konkin³ also investigated the influence of precipitation conditions on the structure and property of *pt*-PSA and poly (3,3'-diphenylsulfonyl terephthalamide) (*mt*-PSA) fibers prepared by wet spinning. Sokira *et al.*⁴ investigated the porous structure changes of PSA fibers during spinning process. It was found that the size and distribution of pores in the as-spun fibers depended on the activity of the precipitant in the precipitation stage. Further, smaller jet, bath, and heat stretching could reduce the porosity of PSA fibers, which is good for the strength improvement. Muraveva *et al.*⁸ found that the *mt*-PSA fibers was amorphous during the forming and cold-drawn process, and intensive crystallization has been formed within the fibers in the heat stretching, contributing to the strength of fibers. Li *et al.*⁹ had systematically studied the effect of drawing ratios on the mechanical property of the final aromatic copolysulfonamide (*co*-PSA) fibers including the jet stretching, plastic stretching, and heat stretching process. The relationship between the molecular orientation and tensile strength has been discussed. In addition, our group has already studied the morphology and structure changes of aromatic copolysulfonamide

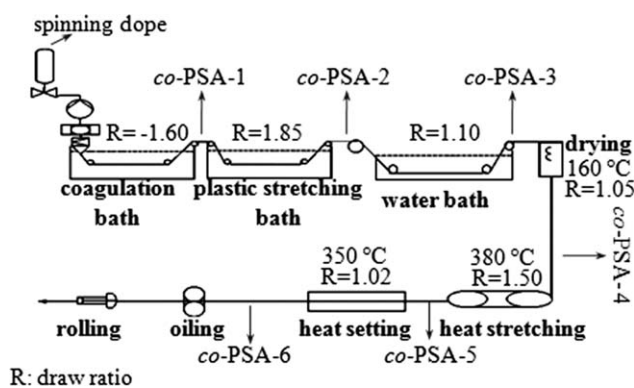


Figure 1. Schematic of wet-spinning process of *co*-PSA fibers.

(*co*-PSA) fibers heat-drawn at various temperatures in our previous work. It has been observed that the mechanical property of *co*-PSA fibers did not follow the conventional increasing mode with the heat drawing temperature, in spite of the substantial improvement in structural perfection.¹⁰

Although separate features of the structure, property, and technology of PSA fibers have been discussed, a systematical analysis of the structure and performance development on spinning line has not been investigated. Some experimental findings indicated that a better understanding of the morphology and structure development of the fibers during spinning process may allow better control of the structure and properties of the final fiber. Ran *et al.*¹¹ investigated the structural development during solution spinning of poly(*p*-phenylenebenzobisoxazole) (PBO) using the in situ synchrotron WAXD and SAXS techniques. The phase transformation from liquid crystal to well-oriented crystals depending on the coagulation time was disclosed. Chen *et al.*¹² studied the structure development of regenerated cellulose fibers during wet spinning process with NaOH/urea as solvent. It was found that drawing of cellulose fiber in the coagulation bath generated higher orientation and crystallinity than drawing in the post treatment.

Although the *co*-PSA fibers have been commercial production, yet the research on the structure and performance related to the spinning process is inadequate. To figure out which stage is the key to the structure development of *co*-PSA fiber, the structure and properties of fiber samples taken from the wet-spinning line were analyzed by SEM, mechanical properties, thermomechanical analyzer (TMA), dynamic mechanical analyzer (DMA), WAXS, and SAXS. Some possible pathways to optimize the spinning technology of *co*-PSA/DMAc solution could be suggested.

EXPERIMENTAL

Materials

The aromatic copolysulfonamide (*co*-PSA) was synthesized via polycondensation of 4,4'-diaminodiphenylsulfone (4,4'-DDS), 3,3'-diaminodiphenylsulfone (3,3'-DDS), and terephthaloyl chloride (TPC) with a monomer mole ratio of 3 : 1 : 4 in *N,N*-dimethylacetamide (DMAc) at 5°C. During the reaction, the right amount of calcium hydroxide (Ca(OH)₂) with the same mole number as DDS was added into the solution to neutralize

hydrogen chloride (HCl) produced in the reaction. The concentrated solution was used as spinning dope directly.

Wet Spinning Process

The *co*-PSA fibers were prepared by using the wet-spinning process sketched in Figure 1. The *co*-PSA spinning dope was filtered and pumped through a spinneret into the coagulation bath, containing DMAc-water (1 : 1 w/w) at 15°C. The as-spun *co*-PSA fibers were drawn in a plastic stretching bath (DMAc-water, 6 : 4 w/w) at 60°C and then subjected to washing, drying, heat stretching, and heat setting.

Characterization

All samples were washed and dried at 105°C under vacuum to constant weight before some tests, including TMA, DMA, and mechanical properties testing.

The cross-section of the *co*-PSA fibers was observed using a scanning electron microscope (SEM, Hitachi S-3000N). The *co*-PSA fibers were cryogenically broken by fiber slicer under liquid nitrogen and were perpendicularly pasted on a sample-carrier, and then sputtered with gold prior to observation.

The stress–strain curves of a single fiber were recorded using a XQ-2 tensile tester with a gauge length of 20 mm and an extension rate of 20 mm/min. At least 50 samples were tested for each samples and the tenacity, elongation at break, and initial modulus were calculated averagely.

Thermomechanical properties of the *co*-PSA fibers were determined on a Hitachi thermal mechanical analyzer (TMA/SS 7100). A single fiber was clamped into the sample holder with a small initial stress in order to keep the fiber straight. The change of fiber length at constant stress (~4.4 MPa) was measured ranging from 40°C to 400°C at 5°C/min.

The dynamic mechanical (DMA) behavior of the *co*-PSA fibers was analyzed using TA Q800 V7.5 instrument to obtain the loss factor ($\tan \delta$). The frequency applied was 1 Hz over a temperature range from 40°C to 400°C at 5°C/min in the temperature-frequency sweeping mode.

Synchrotron X-ray measurements were carried out at Shanghai Synchrotron Radiation Facility (SSRF) on beam line (BL16B) with an X-ray wavelength of 0.124 nm. A bundle of *co*-PSA fibers were put on a sample holder with the fiber direction perpendicular to the X-ray beam. Two types of X-ray measurements were performed respectively: WAXS and SAXS. Two-dimensional (2D) WAXS and SAXS patterns were acquired using a Mar-CCD (165) detector. The sample-to-detector distances for WAXS and SAXS were 169.37 mm and 1910 mm, respectively. All data analysis (background correction, radial, and azimuthal integration) was carried out using the Xpolar software (Precision works NY).

For WAXS analysis, it should be noted that the sharp diffraction peaks come from *d*-spacings in crystallites and rings originate from amorphous regions. Quantitative evaluations of phase fraction were determined from the corrected WAXS patterns, as described by Che *et al.*¹³ and Ran *et al.*¹⁴ The WAXS pattern after correction can be deconvoluted to an isotropic part and anisotropic part using the Xpolar software. The isotropic

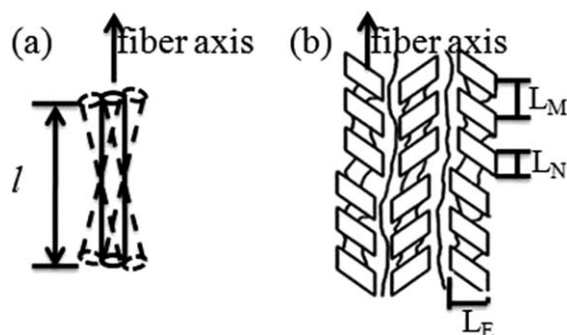


Figure 2. Schematic illustration of the structure corresponding to SAXS patterns.

contribution mainly results from unoriented amorphous component for semi-crystalline *co*-PSA fibers, and the unoriented crystalline component may be ignored. The anisotropic contribution consists of the oriented amorphous (mesophase) and oriented crystalline components. The amorphous fraction is quantitatively determined by taking the ratio of integrated unoriented amorphous peak area (isotropic component) by the total integrated peak area (isotropic and anisotropic component). A 2D peak fit procedure is also applied to separate the crystal phase and mesophase from anisotropic fraction of the scattering.¹⁴ The areas of the crystalline and the mesophase reflections calculated can be used to estimate the fractions of the two different phases in the anisotropic component. Therefore, the relative fraction of crystal, mesomorphic and amorphous phases can be determined.

The crystal orientation (f_a) along the fiber axis was also calculated for the reflections (002) as described in our previous paper.¹⁰

For SAXS analysis, the equatorial streak of small-angle diffuse scattering is generally attributed to the presence of voids or fibrils elongated along the fiber axis.¹⁴ The “needle-shape” model [Figure 2(a)] for *co*-PSA fibers can be adopted and the fibril or micro-voids extends longitudinally along the fiber axis.¹⁵ The average scattering objects length (l) and misorientation angle (B_ϕ) were calculated according to the eq. (1) based on the method of Ruland,¹⁶ as described in the reference.¹⁰

$$sB_{\text{obs}} = l / s + sB_\phi (\text{Cauchy} - \text{Cauchy}) \quad (1)$$

Where s ($s = 2\sin\theta/\lambda$) is the scattering vector, B_{obs} is actually the full width at half maximum of the azimuthal profile from the equatorial streak fitted with a Lorentzian function.

For heat-drawn *co*-PSA fibers, there is detectable four point pattern scattering along the meridional direction, which indicates the existence of lamellar morphology. The structure model for this SAXS pattern can be described as following: the crystalline lamellae within each fibril are separated by interlamellar amorphous chain segments.¹⁷ The schematical presentation was shown in Figure 2(b). Elliptical cylindrical coordinates were found to be best describe the observed small-angle scattering data and the lamellar repeat distance (long period) L_M , lamellae diameter L_E , the lamellae thickness (L_N) were calculated according to the methods proposed by Murthy *et al.*^{18,19}

RESULTS AND DISCUSSION

Morphology of *co*-PSA Fibers Along the Wet Spinning Line

Figure 3 shows the cross section of *co*-PSA fibers along wet spinning line. There was a change in cross-section geometry: the as-spun fibers (*co*-PSA-1) exhibit a waist circle shape cross-section and approach a circle shape after the drying, heat stretching, and heat setting process, which can make up the structural imperfection of *co*-PSA fibers formed in the coagulation. Furthermore, on a smaller scale, it can be found that in the as-spun *co*-PSA fibers the molecules were grouped together in fibrils, which join together to form a three-dimensional fibrillar network. In the following stages, the structure of *co*-PSA fibers became much denser.

Mechanical Properties of *co*-PSA Fibers During Wet Spinning Process

The typical stress-strain curves of all the *co*-PSA samples are shown in Figure 4(1). Figure 4(2) shows the data of mechanical properties, including stress, modulus, and elongation at break. The S-S curves of the fibers exhibit a characteristic behavior with an initially linear section (deformation <3%), a knee at yield point and an approximately linear increase after yielding. Note that the *co*-PSA-1 fibers show a very weak dependence of the stress on the strain after yielding, and the ultimate elongation at break can attain 75% even if it was thoroughly washed and then dried in the vacuum oven. Previous studies^{20,21} showed that PSA molecules are flexible and have random coil

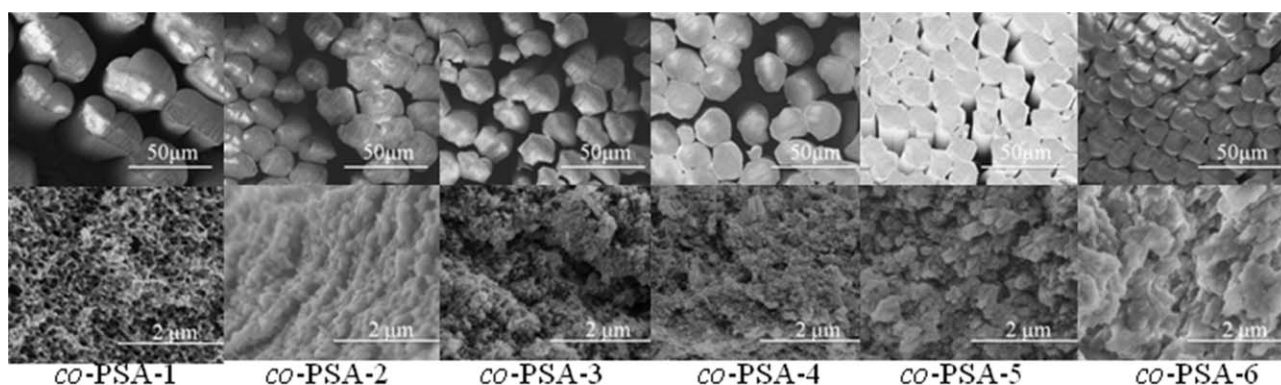


Figure 3. The SEM morphology of cross section of *co*-PSA fibers along the wet spinning line.

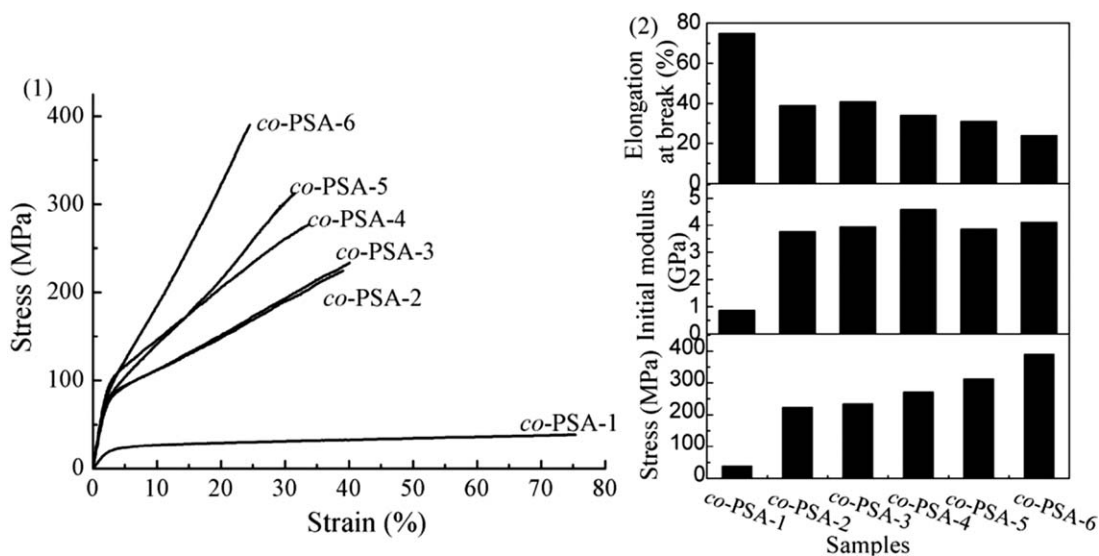


Figure 4. Stress-strain curves (1) and data of mechanical properties (2) of the *co*-PSA fibers along the wet spinning line.

conformations in solution. When the spinning dope was extruded from the spinneret and the as-spun fibers formed with a negative stretching in the coagulation bath, the PSA molecules tend to have lower orientation. Therefore, it exhibited a typical stress-strain behavior like that of semi-crystalline polymer in high-elastic state. When the fibers were subjected to further stretching, heat stretching, and heat setting, the molecules became oriented toward the fiber axis and more dense structure (shown in Figure 3) was formed gradually, which contributed toward the improvement of total strength and modulus along the spinning line.

Thermal Mechanical Analysis of *co*-PSA Fibers During Wet Spinning Process

In order to investigate the thermal stability of *co*-PSA fibers, the TMA analysis was carried out. Figure 5 shows the strain developed in *co*-PSA fibers along the spinning line as they were heated at a constant rate of $5^{\circ}\text{C min}^{-1}$ and under a constant stress of 4.4 MPa. As been expected, the strain was found to be negative since the fibers shrink; otherwise, the fibers are in an extension state. From Figure 5, it can be clearly observed that

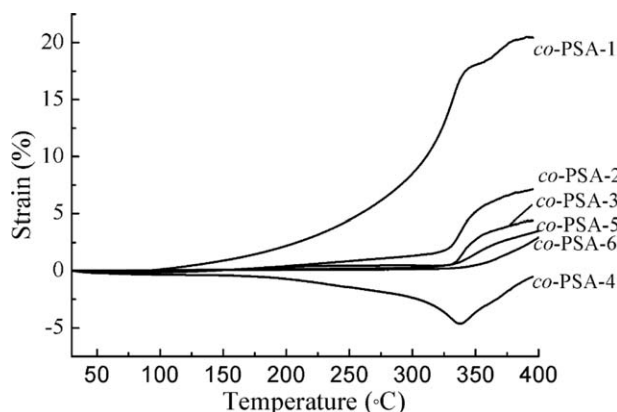


Figure 5. Thermo-mechanical curves of *co*-PSA fibers along wet spinning line.

the strain of all the *co*-PSA fibers had an abrupt change at temperature above 330°C , revealing the start of glass transition of the fibers. In fibers which had not been thermally stretched, especially for *co*-PSA-1~*co*-PSA-3 fibers, another main process took place near 350°C , i.e. at this transition point, considerable crystal structure formed under tension. For the *co*-PSA-5 and *co*-PSA-6 fibers subjected to thermal stretching with a certain crystal structure, this process became unapparent in the thermal mechanical curves. Furthermore, it should be noted that the

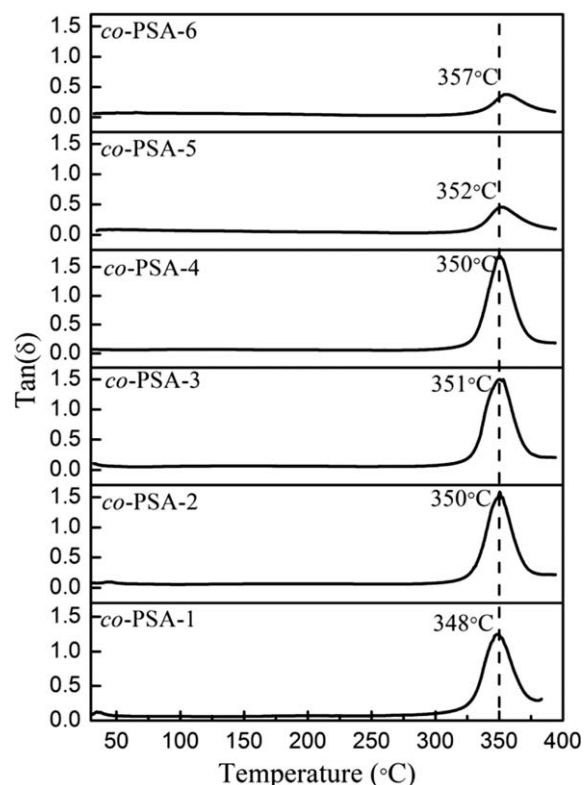


Figure 6. DMA curves of the *co*-PSA fibers along the wet spinning line.

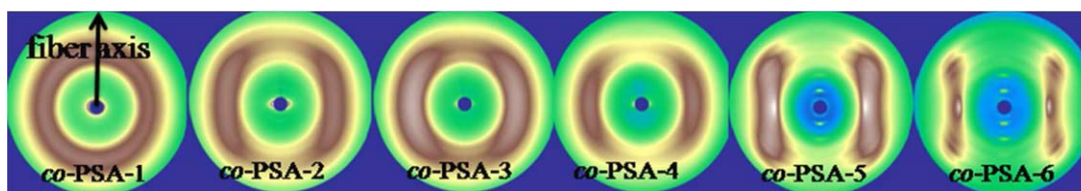


Figure 7. WAXS patterns of the *co*-PSA fibers along the wet spinning line. [Color figure can be viewed in the online issue, which is available at wileyonlinelibrary.com.]

co-PSA-1 fiber had large spontaneous elongation before 300°C. As seen from Figure 3, the *co*-PSA-1 fibers had loose structure, which was helpful to the segmental motion. In the following plastic stretching and washing process, the structure of fibers became much denser; correspondingly, the strain was decreased. However, a shrinkage behavior was observed in *co*-PSA-4 fibers starting from 150°C, which was caused by the large internal stress produced during the drying process. Therefore, it can be found that the structure of *co*-PSA fibers before heat stretching is very unstable. When subjected to heat stretching and heat setting, the crystal structure formed within the fibers contributes to the structure stability, showing no obvious variation in strain before 300°C.

Dynamic Mechanical Analysis of *co*-PSA Fibers During Wet Spinning Process

Figure 6 shows loss factor ($\tan \delta$) of *co*-PSA fibers along the spinning line, which is often used to characterize the motion of chain segments. The $\tan \delta$ curves showed a continuous α transition from 300 to 400°C corresponding to the glass transition of *co*-PSA, which is consistent with the previous paper.²² It is noted that the *co*-PSA fibers displayed almost the same glass transition temperature around 350°C before heat stretching and had similar dynamic thermomechanical behavior according to the $\tan \delta$ -T curves. It indicated that the *co*-PSA fibers had the similar molecular movability in the amorphous regions. Therefore, it can be speculated that similar amorphous structure of *co*-PSA fibers formed before heat stretching although stretching in the coagulation bath and other process conditions before heat stretching can cause certain orientation. Besides, the α transition peak area of *co*-PSA fibers before heat-stretching nearly remained the same, illustrating that these fibers are all in amorphous state. In contrast, it reduced evidently after heat stretching and heat setting process, suggesting that the disordered domain decreased and more ordered and dense phase was formed during this process. Meanwhile, the glass transition temperature of *co*-PSA fibers increased a little after heat setting process.

Microstructure Development of *co*-PSA Fibers Along the Spinning Line

The structure development of *co*-PSA fibers along the spinning line during wet spinning was systematically studied in different length scales.

The amorphous and crystalline structure in nanometer scale was analyzed by WAXS shown in Figure 7. The WAXS pattern of the fibers after coagulation (*co*-PSA-1) exhibited a strong concentric halo, which indicated that only the isotropic amorphous phase existed in the *co*-PSA fiber. In the following spinning stage before heat stretching, the halo tended centralize

along the equator as shown in Figure 7 (*co*-PSA-2~*co*-PSA-4), which shows that only the amorphous state exists within the *co*-PSA fibers and acquires a degree of orientation. The amorphous orientation of these *co*-PSA fibers before heat stretching was determined by Hermans orientation parameter $\langle f_a \rangle$, which can be calculated from the eq. (2) based on the amorphous intensities as a function of the azimuthal angle (as shown in Figure 8).²³

$$f_a = (3\langle \cos^2 \phi \rangle - 1) / 2$$

$$\langle \cos^2 \phi \rangle = \frac{\int_0^\pi \cos^2 \phi \sin \phi I \phi d\phi}{\int_0^\pi \sin \phi I \phi d\phi} \quad (2)$$

Where $I(\phi)$ is the total height of the amorphous scattering at ϕ . The f_a values for the various *co*-PSA fibers are tabulated in Table I. As seen from the Table I, the orientation of PSA molecules before heat stretching process occurred mainly in the plastic stretching stage.

Noticeably, the significant structural conversions of *co*-PSA fibers occurred after heat stretching. In Figure 7 (*co*-PSA5 and 6), the equatorial, meridional reflections and the presence of

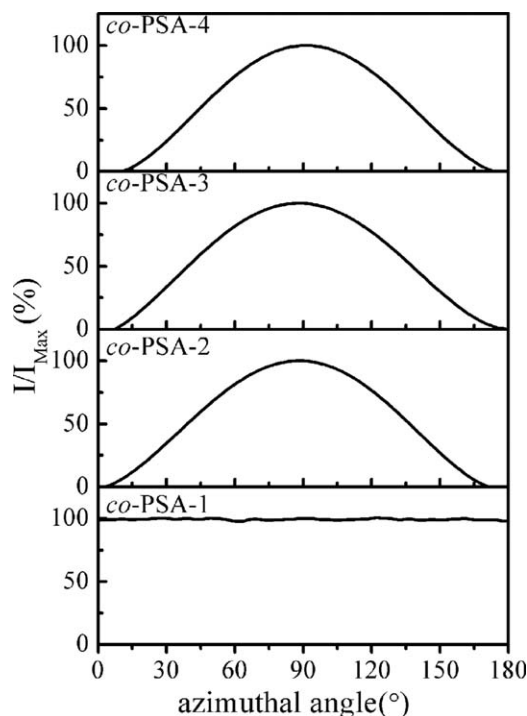
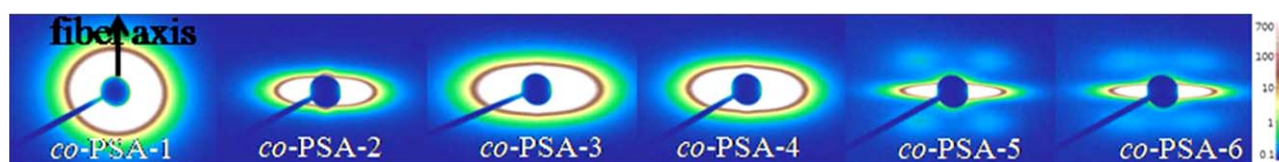


Figure 8. Relative intensity distribution along azimuthal angle (ϕ) of the amorphous phase region of *co*-PSA fibers.

Table I. Structural Parameters of *co*-PSA Fibers Along the Wet Spinning Line

	<i>co</i> -PSA-1	<i>co</i> -PSA-2	<i>co</i> -PSA-3	<i>co</i> -PSA-4	<i>co</i> -PSA-5	<i>co</i> -PSA-6
Amorphous fraction (%)	100	89	87	85	58	44
Mesophase fraction (%)	0	11	13	15	22	26
Crystal fraction (%)	0	0	0	0	20	30
amorphous orientation f_a	0.00	0.40	0.37	0.38	–	–
Crystal orientation f_c	–	–	–	–	0.94	0.95

**Figure 9.** SAXS patterns of the *co*-PSA fibers along the wet spinning line. [Color figure can be viewed in the online issue, which is available at wileyonlinelibrary.com.]

off-axis (hkl) reflections developed following the heat stretching and became sharper after heat setting, indicating that the development of crystalline structure within the fibers. In order to illustrate the structure development along the spinning line explicitly, a two-dimensional image analysis method as described by Che *et al.*¹³ and Ran *et al.*¹⁴ was used to extract quantitative information of crystal, amorphous, and mesomorphic fractions from 2D WAXS patterns, as listed in Table I. It is seen that the 100% of the amorphous fraction in the *co*-PSA-1 fibers suggested that the fibers formed in coagulation were completely in amorphous states. In the plastic stretching process, some of amorphous phase can be converted to the mesophase, which indicate that some chains had only one or 2D ordering and pack along the fiber axis. It is noted that the variations of the mass fraction in the amorphous phase and mesophase were relatively small in the washing and drying process because the deformation employed small stretch ratios. When the fibers were subjected to heat stretching, the fraction for the amorphous phase decreased obviously and that for mesophase increased. The crystallites were found to form during this process. After heat setting, the ordered phase content further increased and the crystal orientation can reach up to 0.95. The structural conversion from disordered state to order is beneficial for the improvement of mechanical properties of fibers.

The analysis for the microstructure of the *co*-PSA fibers at large scale was done by SAXS as shown in Figure 9. The circular scat-

tering halo was seen for *co*-PSA-1 fibers, indicating a random orientation structure formed within the fibers. In the following process, the fibers showed intense diffuse scattering along the equator in the SAXS pattern, especially for *co*-PSA fibers after heat stretching, the equatorial streak became sharper and grew in intensity, which suggested that higher orientation structure has been formed with respect to the fiber axis. It should also be noted that the SAXS pattern of *co*-PSA fibers after heat stretching shows a four point pattern scattering along the meridian, which indicates the existence of periodic lamellar morphology.²⁴

Quantitative analysis for SAXS such as the size of scattering objects (fibril or voids) and lamellae as schematized in Figure 2 was also conducted. To determine the scattering objects caused the streak along the equator in SAXS, the wet *co*-PSA fibers (soak the fibers in water for 1 h and suck the surface water of fibers by filter paper) were used for SAXS experiments, as reported in our previous study.¹⁰ As expected, the presence of moisture markedly reduced the intensity of the equatorial scatter of *co*-PSA fibers before heat stretching, especially for wet *co*-PSA-0 fibers, the intensity almost disappeared. In contrast, the wet *co*-PSA fibers after heat stretching had a little loss in intensity. The changes in intensity can be explained in terms of uptake of water reducing inherent electron density differences within the fibers. From Figure 3, it can be seen that the *co*-PSA fibers have more dense structure along the spinning line, particularly forming the crystal structure after heat stretching.

Table II. The Average Length (l) of the Scattering Objects, Misorientation Angle (B_ϕ), and Lamellar Structure Parameters of *co*-PSA Fibers

	<i>co</i> -PSA-1	<i>co</i> -PSA-2	<i>co</i> -PSA-3	<i>co</i> -PSA-4	<i>co</i> -PSA-5	<i>co</i> -PSA-6
B_ϕ (°)	77.1	34.2	48.2	43.7	11.9	10.5
l (nm)	243.0	–	–	–	1035.0	596.0
L_M (mn)	–	–	–	–	20.7	21.1
L_E (mn)	–	–	–	–	4.4	6.8
L_N (mn)	–	–	–	–	14.5	15.3

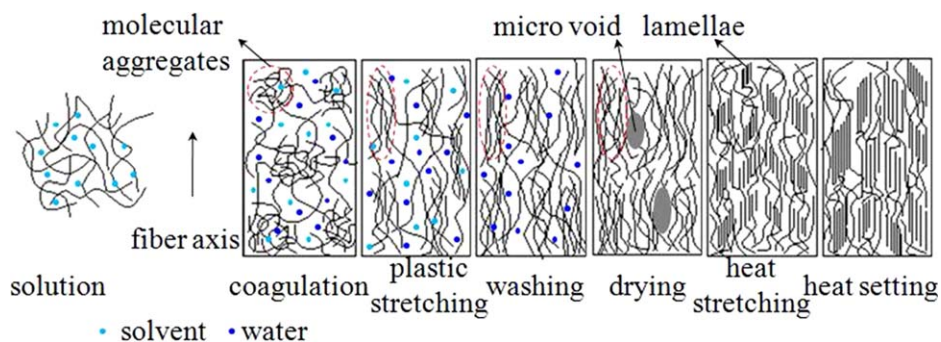


Figure 10. Schematic structural models of *co*-PSA fibers during spinning process. [Color figure can be viewed in the online issue, which is available at wileyonlinelibrary.com.]

Therefore, it is reasonable to deduce that the slight change in intensity of heat stretching and heat setting *co*-PSA fibers is mainly due to the absorption of water in disordered regions. On the contrary, this may imply the presence of voids within the fibers before heat stretching. It could be easily concluded that the scattering objects in the *co*-PSA fibers after heat stretching mainly associated with the microfibrillar structure, while those in the fibers before heat stretching may be related with the combined effect of voids and fibrils. Therefore, based on the SAXS pattern, the average length l and misorientation angle B_ϕ of scattering objects can be determined by the method of Ruland,¹⁶ as listed in Table II. The misorientation of scattering objects tends to decrease along the spinning line. These results suggest that the orientation of *co*-PSA molecules occurred mainly in the plastic stretching and heat stretching stage, which is consistent with the results of WAXS. In addition, it can be found that the average length within the *co*-PSA-0 fibers is about 243 nm. For *co*-PSA-2~*co*-PSA-4 fibers, the fit curve gives a negative intercept, which illustrated that the objects are larger enough, over a certain length, which result from the uniaxial tension in the spinning stage. However, the object (fibril) length of *co*-PSA fibers decreased in the heat stretching and setting stages. It is mainly because the PSA chain segments are inclined to pack into crystal lattice with a big Zig-Zag conformation in these processes.¹⁰ The lamellar structure of *co*-PSA fibers after heat setting tends to improve with large size as list in Table II.

To visualize the changes in structure during processing, an appropriate structural model was also proposed, as shown in Figure 10. As stated in previous article,^{20,21} the PSAs have random coil conformations in solution. When the *co*-PSA spinning dope was extruded through the spinnerets into coagulation bath, the molecules of *co*-PSA were arranged in fibrils and formed a three-dimensional random network during coagulation; during plastic stretching process, the network tends to deform along the stretching direction and the orientation of molecular aggregates was found to increase obviously. In the washing and drying process, the orientation of *co*-PSA fibers changed a little, but the solvent and water was removed and the structure of fibers became much denser. After heat stretching, the four point teardrop pattern with diagonal orientation of teardrops indicated the lamellar tilting persisted.²⁵ As mentioned above, the lamellar structure was found to grow in size during the heat setting process.

CONCLUSIONS

The structure and performance changes of aromatic copolysulfonamide (*co*-PSA) fibers that occurred during wet spinning process were discussed. During the first coagulation, phase separation occurred within the *co*-PSA filaments and the molecules were arranged to form random network. Correspondingly, the *co*-PSA fibers were found to exhibit good extensibility but low strength. During the following plastic stretching process, the primary deformation process involved the molecular arrangement from disordered state (amorphous) to one or 2D ordering and pack along the fiber axis (mesophase). In the washing and drying process, the solvent and water was removed respectively. The structure of *co*-PSA fibers became much denser during these processes, but the amorphous orientation was almost unchanged. The *co*-PSA fibers before heat stretching were unstable. When the *co*-PSA fibers were heat stretched at the temperature higher than T_g , the crystal structure formed within the fibers and became more perfect after heat setting, which contributed to the improvement of structural stability and mechanical properties.

ACKNOWLEDGMENTS

This work was financially supported by National Natural Science Foundation of China (11079015 and 51273039) and Chinese Universities Scientific Fund (CUSF-DH-D-2014024).

REFERENCES

1. Wang, X.; Zhang, Y. *China Textile Leader* **2005**, *1*, 18 (Chinese).
2. Ban, Y.; Zhang, Y.; Ren, J. *Tech. Text.* **2006**, *12*, 33 (Chinese).
3. Muraveva, N. I.; Konkin, A. A. *Fibre Chem.* **1971**, *3*, 612.
4. Sokira, A. N.; Efimova, S. G.; Shchetinin, A. M.; Frenkel, G. G.; Iovleva, M. M. *Fibre Chem.* **1979**, *10*, 545.
5. Zhang, Y.; Wang, H.; Chen, S.; Wang, X.; Fang, D.; Burger, C.; Che, J.; Li, X.; Hsiao, B. S. *Macromol. Chem. Phys.* **2013**, *214*, 2432.
6. Banduryan, S. I.; Ivanova, N. A.; Efimova, S. G.; Sokira, A. N.; Shchetinin, A. M.; Frenkel, G. G.; Budnitskii, G. A.; Iovleva, M. M. *Fibre Chem.* **1978**, *9*, 484.

7. Banduryan, S. I.; Shchetinin, A. M.; Grechishki, A. V.; Lovleva, M. M.; Papkov, S. P. *Fibre Chem.* **1976**, *7*, 631.
8. Muraveva, N. I.; Konkin, A. A. *Fibre Chem.* **1973**, *4*, 127.
9. Li, H.; Wang, X.; Xu, B.; Chen, S.; Peng, X.; Zhang, Y.; Zhao, J. *Synth. Technol. Appl.* **2013**, *28*, 1 (Chinese).
10. Yu, J.; Wang, R.; Yang, C.; Chen, S.; Tian, F.; Wang, H.; Zhang, Y. *Polym. Int.* **2014**, *63*, 2084.
11. Ran, S.; Burger, C.; Fang, D.; Zong, X.; Cruz, S.; Chu, B.; Hsiao, B. S.; Bubeck, R. A.; Yabuki, K.; Teramoto, Y.; Martin, D. C.; Johnson, M. A.; Cunniff, P. M. *Macromolecules* **2002**, *35*, 433.
12. Chen, X.; Burger, C.; Wan, F.; Zhang, J.; Rong, L.; Hisao, B. S.; Chu, B.; Cai, J.; Zhang, L. *Biomacromolecules* **2007**, *8*, 1918.
13. Che, J.; Locker, C. R.; Lee, S.; Rutledge, G. C.; Hsiao, B. S.; Tsou, A. H. *Macromolecules* **2013**, *46*, 5279.
14. Ran, S.; Fang, D.; Zong, X.; Hsiao, B. S.; Chu, B.; Cunniff, P. M. *Polymer* **2001**, *42*, 1601.
15. Jiang, G.; Huang, W.; Li, L.; Wang, X.; Pang, F.; Zhang, Y.; Wang, H. *Carbohydr. Polym.* **2012**, *87*, 2012.
16. Ruland, W. J. *Polym. Sci.: Part C* **1969**, *28*, 143.
17. Murthy, N. S.; Bednarczyk, C.; Moore, R. A. F.; Grubb, D. T. *J. Polym. Sci. Pol. Phys.* **1996**, *34*, 821.
18. Murthy, N. S.; Grubb, D. T. *J. Polym. Sci. Pol. Phys.* **2006**, *44*, 1277.
19. Murthy, N. S.; Grubb, D. T.; Zero, K. *Macromolecules* **2000**, *33*, 1012.
20. Chen, Y.; Wu, D.; Li, J.; Chen, S.; Wang, X.; Zhang, Y.; Wang, H. *Macromol. Symp.* **2010**, *298*, 116.
21. Prozorova, G. E.; Pavlov, A. V.; Shchetinin, A. M.; Iovleva, M. M.; Papkov, S. P. *Vysokomolekulyarnye Soedineniya, Seriya B: Kratkie Soobshcheniya* **1977**, *19*, 750 (Russian).
22. Kuznetsov, G. A.; Nikiforov, N. I.; Lebedev, V. P.; Zhuravlev, V. G.; Savinov, V. M. *Vysokomol. Soyed.* **1974**, *16*, 2711.
23. Murthy, N. S.; Bednarczyk, C.; Rim, P. B.; Nelson, C. J. *J. Appl. Polym. Sci.* **1997**, *64*, 1363.
24. Pope, D. P.; Keller, A. *J. Polym. Sci. Pol. Phys.* **1975**, *13*, 533.
25. Fakirov, S.; Fakirov, C.; Fischer, E. W.; Stamm, M.; Apostolov, A. A. *Colloid Polym. Sci.* **1993**, *271*, 811.